Hindawi
Wireless Communications and Mobile Computing
Volume 2017, Article ID 4361589, 7 pages
https://doi.org/10.1155/2017/4361589

Research Article

Influence of Pulse Shaping Filters on PAPR Performance of Underwater 5G Communication System Technique: GFDM

Jinqiu Wu,[1,2] Xuefei Ma,[1] Xiaofei Qi,[1] Zeeshan Babar,[1] and Wenting Zheng[1]

[1]*College of Underwater Acoustic Engineering, Harbin Engineering University, Harbin 150001, China*
[2]*College of Communication and Electronic Engineering, Qiqihar University, Qiqihar 161000, China*

Correspondence should be addressed to Xuefei Ma; xuefeima@163.com

Received 8 December 2016; Revised 19 January 2017; Accepted 15 February 2017; Published 28 February 2017

Academic Editor: Yoshikazu Miyanaga

Generalized frequency division multiplexing (GFDM) is a new candidate technique for the fifth generation (5G) standard based on multibranch multicarrier filter bank. Unlike OFDM, it enables the frequency and time domain multiuser scheduling and can be implemented digitally. It is the generalization of traditional OFDM with several added advantages like the low PAPR (peak to average power ratio). In this paper, the influence of the pulse shaping filter on PAPR performance of the GFDM system is investigated and the comparison of PAPR in OFDM and GFDM is also demonstrated. The PAPR is restrained by selecting proper parameters and filters to make the underwater acoustic communication more efficient.

1. Introduction

The bandwidth limitation of underwater acoustic (UWA) channel makes OFDM one of the most significant and widely used modulation techniques for UWA communication. Although OFDM has considerable advantages over single-carrier modulations in combating frequency selective fading, it does not suit well with the future requirements because of the need for precise synchronization and the large PAPR. The requirement for cyclic prefix (CP) in every OFDM symbol also limits its spectral efficiency. Consequently, new multicarrier transmission schemes are needed to address these problems. Among them, filter bank multicarrier (FBMC) [1] and generalized frequency division multiplexing (GFDM) [2] are new promising techniques for 5G applications. GFDM is a two-dimensional (time and frequency) block-based data structure with multicarrier transmission scheme that is also derived from the filter bank approach [3, 4]. It divides the transmitting data into subgroups and subcarriers and each subcarrier is pulse shaped with prototype filter. This process reduces the OOB emissions and PAPR, making fragmented spectrum and dynamic spectrum allocation feasible without severe interference in incumbent services or other users [5].

It is a novel concept for flexible multicarrier transmission that introduces additional degrees of freedom when compared to traditional OFDM [6]. The CP insertion method of GFDM is different from OFDM, where CP is added in each block instead of each symbol, which increases the efficiency of the system.

The flexibility of GFDM allows it to cover a single-carrier frequency domain equalization (SC-FDE) and CP-OFDM as special cases [5–7]. When $M = 1$ and the filter bank $A = F_N^H$, where F_N is a $N \times N$ Fourier matrix and F^H is the Hermitian transpose of F, GFDM turns into OFDM. When $K = 1$ and $\vec{g}$ is a Dirichlet pulse SC-FDE is obtained. Thus, GFDM retains all main benefits of OFDM at the cost of some additional implementation complexity. The block structure of GFDM can be designed according to requirements, especially for the bandwidth limited system. The flexibility of the selection in the number of subblocks and subcarriers makes GFDM utilize fragmented spectrum which greatly increases the spectrum efficiency. These aspects are relevant for the scheduling of users in a multiple access scenario [8]. One of the main advantages of GFDM over OFDM is the low PAPR [9]. The PAPR character is one of the most important parameters to measure the performance of GFDM communication system.

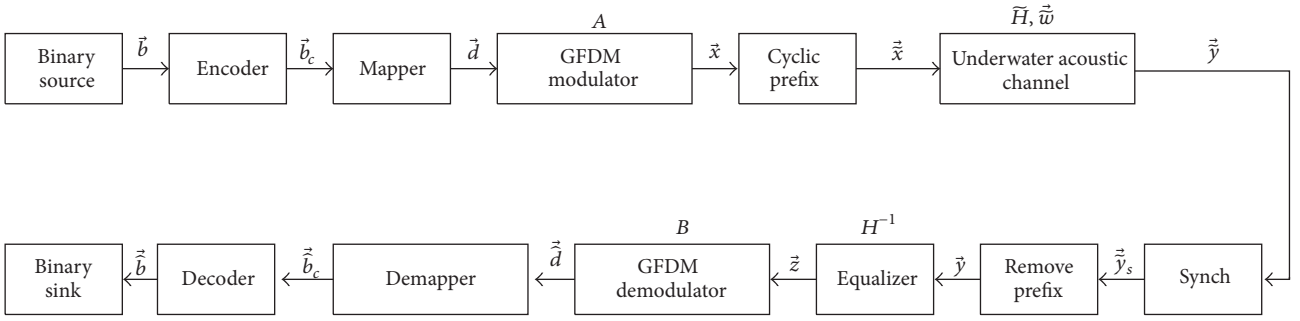

Figure 1: Block diagram of the transceiver.

References [7–9] that have been published focus on the BER performance of GFDM, while there has been no systematic research on the PAPR performance of GFDM. Based on this, the paper gives a systematical analysis and it is an important reference for further application of this technique about how to select the appropriate filter banks and parameters according to the linear dynamic range of the transmitter power amplifier especially for the band limited underwater communication field.

The rest of this paper is organized as follows. In Section 2, a typical GFDM system and its properties are demonstrated including the bock diagram, PAPR of GFDM, and pulse shaping filters used in GFDM system. Then, simulation results of the influence of the pulse shaping filter on PAPR are analyzed in Section 3. Finally, conclusions are drawn in Section 4.

2. System Model and Properties

2.1. Sending Terminal. The block diagram of GFDM communication system is shown in Figure 1. Vector $\vec{b}_c$ is the decoded data of the original binary data $\vec{b}$, while after modulation we obtain vector $\vec{d}$. The dimension of $\vec{d}$ is $N \times 1$ and it can be decomposed into K subcarriers with M subsymbols, which satisfies the equation $N = K \times M$. Vector $\vec{d}$ can be expressed as $\vec{d} = (\vec{d}_0^T, \ldots, \vec{d}_{M-1}^T)^T$, where $\vec{d}_0 = (\vec{d}_{0,0}^T, \ldots, \vec{d}_{K-1,0}^T)^T$ and $\vec{d}_m = (\vec{d}_{0,m}^T, \ldots, \vec{d}_{K-1,m}^T)^T$. Therefore, $d_{k,m}$ is the data transmitting on the kth subcarrier and mth subsymbol of the block.

$$g_{k,m}[n] = g[(n - mK) \bmod N] \cdot \exp\left[-j2\pi \frac{k}{K} n\right], \quad (1)$$

where n denotes the sampling index. From (1), we can see that each $g_{k,m}[n]$ is the different time and frequency transformation of prototype filter $g[n]$.

The transmitting data $\vec{x} = (x[n])^T$ can be superimposed by all sending symbols.

$$x[n] = \sum_{k=0}^{K-1} \sum_{m=0}^{M-1} g_{k,m}[n] \cdot d_{k,m}, \quad n = 0, \ldots, N-1. \quad (2)$$

Let $\vec{g}_{k,m} = (g_{k,m}[n])^T$; (2) can be [8]

$$\vec{x} = A\vec{d}, \quad (3)$$

where the dimension of A is $KM \times KM$ and can be expressed as

$$A = \left(\vec{g}_{0,0} \cdots \vec{g}_{K-1,0} \vec{g}_{0,1} \cdots \vec{g}_{K-1,M-1}\right), \quad (4)$$

where $\vec{g}_{k,m}$ is the time and frequency shifted version of $\vec{g}_{0,0}$. Finally, after adding CP, the sending signal can be expressed as $\vec{\tilde{x}}$, which is the GFDM modulated data $\vec{d}$. $\vec{g}_{1,0} = [A]_{n,2}$ and $\vec{g}_{0,1} = [A]_{n,K+1}$ are circularly frequency and time shifted versions of $\vec{g}_{0,0} = [A]_{n,1}$. The GFDM modulator is shown in Figure 2. Each $d_{k,m}$ is transmitted with the corresponding pulse shape $g_{k,m}$.

2.2. Receiving Terminal. Transmission though underwater channel can be modeled by

$$\vec{y} = H\vec{x} + \vec{w}, \quad (5)$$

where $\vec{y}$ is the receiving signal, $\vec{x}$ is the sending signal, the underwater channel matrix is H, and $\vec{w}$ denotes the additive white Gaussian noise (AWGN). At the receiver, time and frequency synchronization are performed and cyclic prefix is removed. Under the assumption of perfect synchronization, channel equalization used in OFDM can be adopted in GFDM.

The dimension of channel matrix H is $N \times N$. After channel estimation and equalization, the receiving signal is represented by $\vec{z}$ as

$$\vec{z} = H^{-1}\vec{y} + \vec{w} = H^{-1}HA\vec{d} + H^{-1}\vec{w} = A\vec{d} + \overrightarrow{\tilde{w}}. \quad (6)$$

After GFDM demodulation, the estimated data will be

$$\vec{\hat{d}} = B\vec{z}. \quad (7)$$

The dimension of matrix B is $KM \times KM$; the form of B will be different when using different equalization method such as (match filter) MF, (zero forcing) ZF, and (Minimum Mean Square Error) MMSE. The forms of B are given as follows:

$$\begin{aligned} B_{\mathrm{MF}} &= A^H, \\ B_{\mathrm{ZF}} &= A^{-1}, \\ B_{\mathrm{MMSE}} &= \left(\frac{\sigma_n^2}{\sigma_d^2} I + A^H A\right)^{-1} A^H, \end{aligned} \quad (8)$$

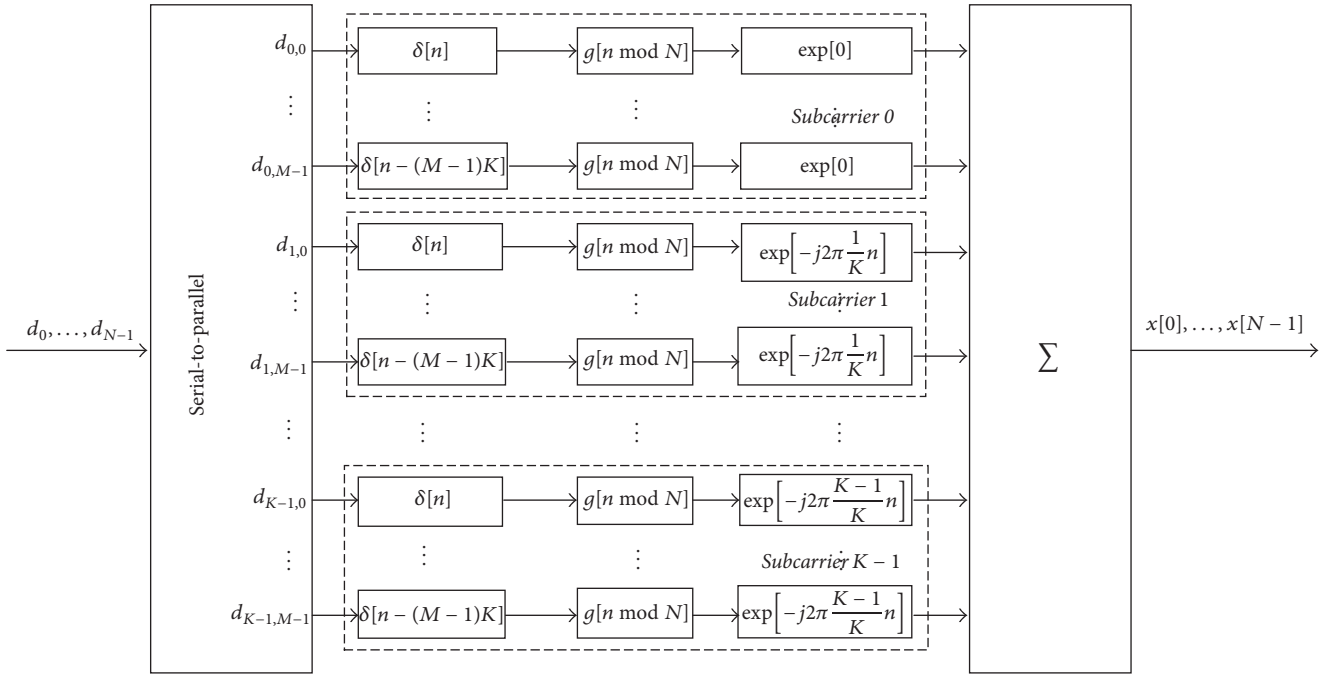

Figure 2: Modulator of the GFDM.

where σ_n^2 and σ_d^2 are noise and signal variance. After demodulation and decoding, we get the estimated binary data $\overrightarrow{\hat{b}}$.

Figure 1 shows the block diagram of GFDM in underwater acoustic communication system. In the first step, the source data vector $\vec{b}$ is encoded as $\vec{b}_c$, followed by GFDM modulator, which modulates mapped data $\vec{d}$. The detailed structure of modulator is shown in Figure 2. The GFDM modulator plays a similar role as IFFT in OFDM. Vector $\vec{d}$ is the data block with dimension $N \times 1$, which is composed of K subcarriers and M subsymbols and N satisfies the equation $N = K \times M$. After adding CP to the modulated data $\vec{x}$, the data $\overrightarrow{\tilde{x}}$ is transmitted through the underwater acoustic channel. At the receiving terminal the channel estimation and equalization are performed after synchronization and CP removal. Finally, the estimated sending data $\overrightarrow{\hat{b}}$ is obtained after demapping and decoding.

From the description of the sending and receiving terminal, it can be concluded that GFDM falls into the category of filtered multicarrier systems [10–12]. The name derives from the fact that the scheme offers more degrees of freedom than traditional OFDM or single carrier with SC-FDE.

Figure 2 shows the modulator of GFDM, in which $d_{k,m}$ represents data transmitted on the kth subcarrier and, in the mth subsymbol of the block, pulse shaped by the corresponding pulse shape filter $g_{k,m}$. Time and frequency division of OFDM, SC-FDE, and GFDM are shown in Figure 3. From Figure 3, we can conclude that GFDM is the generalization of OFDM and SC-FDE. When $M = 1$ and $K = N$ GFDM turns into OFDM and whenever $M = N$ and $K = 1$ SC-FDE is obtained. Consequently, the PAPR of GFDM will range between OFDM and SC-FDE.

2.3. PAPR of GFDM. A discrete GFDM signal is given in

$$\overrightarrow{\tilde{x}}(n) = \sum_{k=0}^{K-1} \sum_{m=0}^{M-1} g_{k,m}[n]\, d_{k,m} e^{-j(2\pi nk/K)}, \tag{9}$$

where $K \times M = N$ and $g_{k,m}[n] = g[(n - mk) \bmod N] \cdot \exp[-j2\pi(k/K)n]$ is the time and frequency conversion of prototype filter $g[n]$. $d_{k,m}$ represents data on the kth subcarrier in the mth subsymbol of the block. In each block, M signals superimposed on M carriers to produce the GFDM waveform. M signals in one subsymbol block overlap with the same phase; GFDM signals will confront a peak power which is M times larger than the average power. Therefore, the PAPR of GFDM signal is expressed as

$$\text{PAPR (dB)} = 10 \log_{10} \frac{\max_{0 \le n \le N-1} \left[|x_n|^2 \right]}{E\left[|x_n|^2 \right]}, \tag{10}$$

where $E[\cdot]$ is mathematical expectation and x_n represents the discrete GFDM signal in time domain. From expression (9), the amplitude of the GFDM signal can be expressed as

$$A(n) = \sqrt{\text{Re}^2\{x(n)\} + \text{Im}^2\{x(n)\}}. \tag{11}$$

The cumulative distribution function can be written as

$$F(z) = 1 - e^{-z}. \tag{12}$$

The complementary cumulative distribution function (CCDF) can be defined as

$$\begin{aligned} P(\text{PAPR} > z) &= 1 - P(\text{PAPR} \le z) = 1 - F(z)^N \\ &= \left(1 - e^{-z}\right)^N. \end{aligned} \tag{13}$$

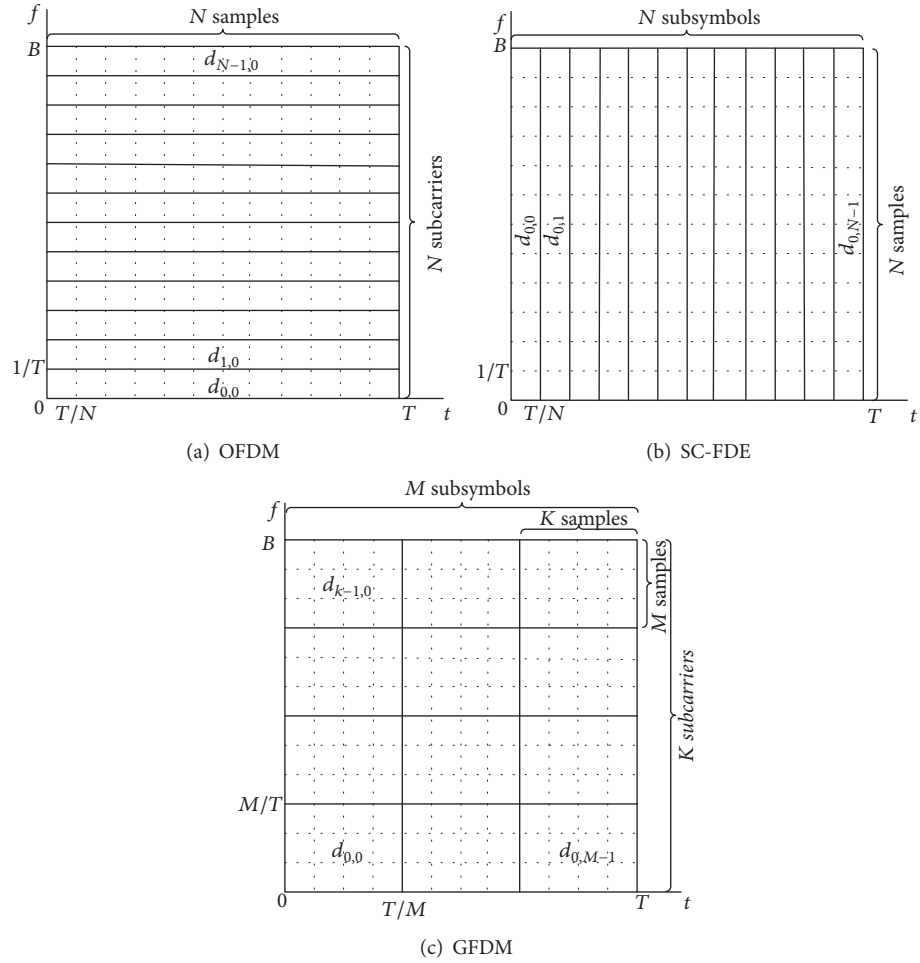

Figure 3: Time and frequency division of different system.

CCDF is a curve to measure the distribution of system's PAPR. The PAPR is influenced by many factors of pulse shaping filter used in GFDM communication system.

2.4. Pulse Shaping Filter. The frequency response of pulse shaping filters can be used in GFDM system which are shown in Table 1 [13, 14], in which $\mathrm{lin}_\alpha(x)$ is a truncated linear function.

$$\mathrm{lin}_\alpha(x) = \min\left(1, \max\left(0, \left(\frac{1+\alpha}{2\alpha} + \frac{|x|}{\alpha}\right)\right)\right). \quad (14)$$

Equation (14) is used systematically to describe the roll-off area defined by α in frequency domain. And $p_4(x) = x^4(35 - 84x + 70x^2 - 20x^3)$ is a polynomial that maps the range $(0, 1)$ onto itself.

Table 1: Frequency response of different filters.

Name	Frequency response
RC	$G_{\mathrm{RC}}[f] = \frac{1}{2}\left[1 - \cos\left(\pi \mathrm{lin}_\alpha\left(\frac{f}{M}\right)\right)\right]$
RRC	$G_{\mathrm{RRC}}[f] = \sqrt{G_{\mathrm{RC}}[f]}$
1st Xia	$G_{\mathrm{Xia1}}[f] = \frac{1}{2}\left[1 - \exp\left(-j \mathrm{lin}_\alpha\left(\frac{f}{M}\right)\mathrm{sign}(f)\right)\right]$
4th Xia	$G_{\mathrm{Xia4}}[f] = \frac{1}{2}\left[1 - \exp\left(-j\pi p_4\left(\mathrm{lin}_\alpha\left(\frac{f}{M}\right)\right)\mathrm{sign}(f)\right)\right]$

3. Simulation Results Analysis

OFDM and GFDM UWA communication system's parameters are shown in Table 2.

The sample frequency of the system is 48 kHz and the bandwidth of OFDM signal is $B = 6$ kHz. The transmitted signal occupies the frequency band between 6 kHz and 12 kHz. We use cyclic-prefixed OFDM and GFDM with a cycle-prefix $Tg = 20.8$ ms per OFDM block. The setting of cycle-prefix is according to the maximum multipath delay of the underwater channel which generally ranges from 10 ms to 20 ms. BPSK modulation is used. The signal parameters are summarized in Table 2.

Figure 4 is the frequency domain of 1st Xia, 4th Xia, RC (Raised Cosine), and RRC (Root Raised Cosine) shaping filters with the roll-off factor α equal to 0.1 and 0.9. From the

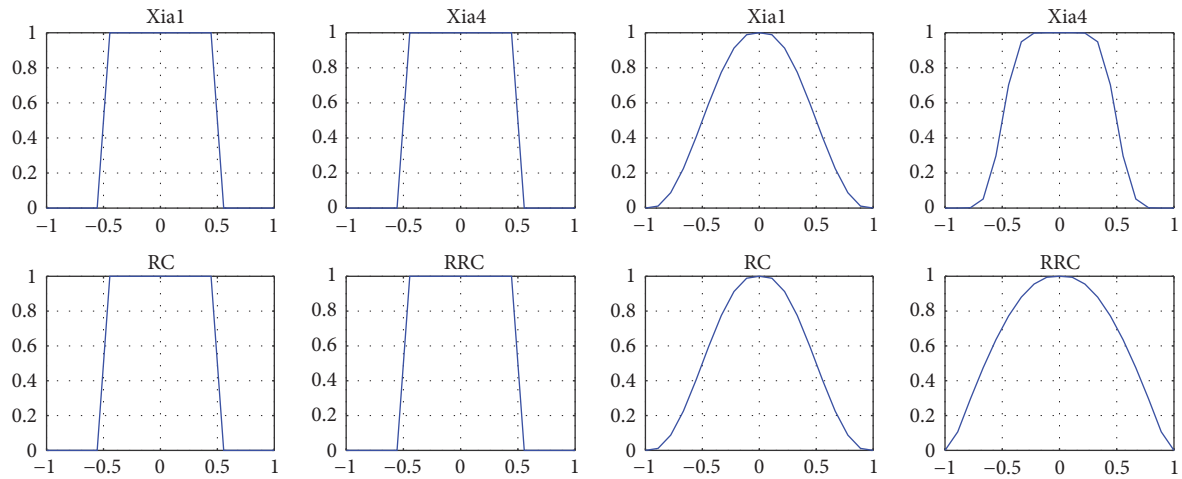

Figure 4: The frequency domain of 4 pulse shaping filters with α 0.1 and 0.9.

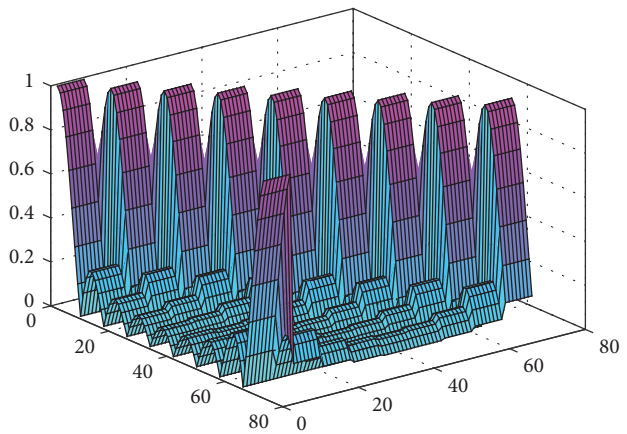

Figure 5: Value of matrix A with $\alpha = 0.1$, $K = 8$, and $M = 9$.

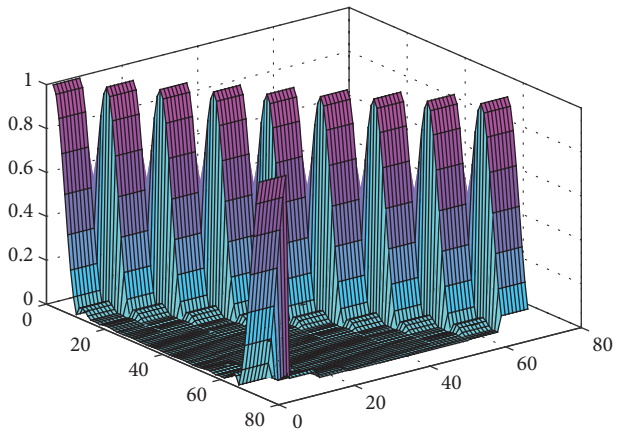

Figure 6: Value of matrix A with $\alpha = 0.9$, $K = 8$, and $M = 9$.

Table 2: Simulation parameter.

Parameter	Value
Signal modulation type	BPSK
The cyclic prefix length	20.8 ms
The sample frequency	48 kHz
Bandwidth	6 kHz
Starting frequency	6 kHz

picture, we can draw the conclusion that when α is 0.1, the frequencies of the four filters are almost the same. When α approach 0.9, their performances become different. Figures 5 and 6 are the value of the matrix A with the roll-off factor $\alpha = 0.1$ and 0.9. From Figures 4, 5, and 6, we can draw the conclusion that with the increase of α the side lobe of the filter bank becomes lower. Figure 6 shows the detailed influence of pulse shaping filters on PAPR performance.

Figure 7 shows the comparison of the CCDF of OFDM and GFDM communication systems for the same transmitted data. The complementary cumulative distribution function (CCDF) is one of the most frequently used parameters for analyzing PAPR reduction by measuring its distribution.

GFDM is a block structure with the dimensions $M \times K$, where M is the subblock number and K is the subcarrier number. Simulations are performed for different number of subcarriers of GFDM including 516, 258, 129, and 8. Figure 7 proves that GFDM has less PAPR than OFDM for the same parameters; for example, for CCDF less than 0.2, the PAPR of OFDM is larger than GFDM by 17.5 dB when the subcarrier number is 8 and the subblock number is 129. In order to keep the same transmitting data bits, there are 8 subblocks for 129 subcarriers and the PAPR of GFDM is about 9 dB lower than OFDM. When the number of subcarriers is 258 and the corresponding number of subblocks is 4, the PAPR of GFDM is about 7 dB lower than that of OFDM and about 2 dB higher than the scenario when the number of subcarriers is 129. When the number of subcarriers rises to 516, the PAPR of GFDM rises to 30 dB which is still 3 dB lower than OFDM. The influence of different filters on PAPR is depicted in Table 1, while Figure 8 shows the influence of the filters on PAPR. The comparison is based on the condition that

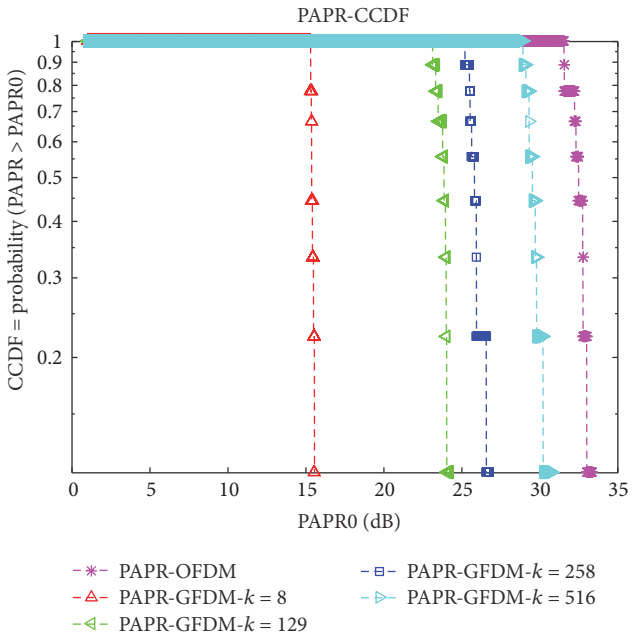

Figure 7: CCDF of OFDM and GFDM communication system with different number of subcarriers.

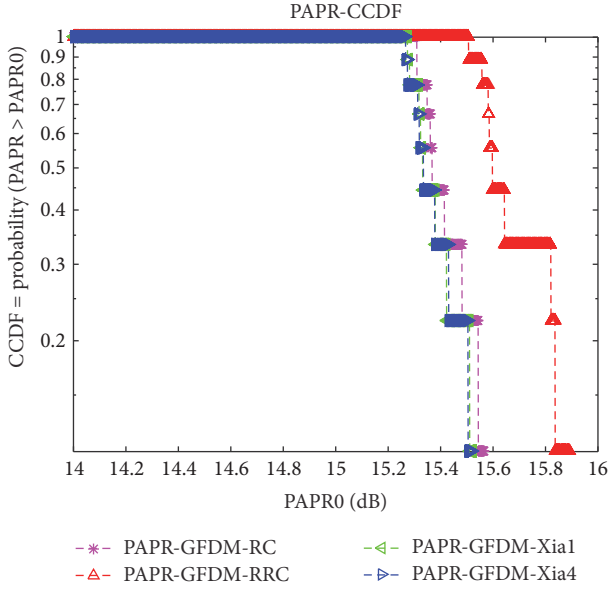

Figure 8: CCDF of GFDM communication system with different filters.

the number of subcarriers in different systems is the same. Figure 8 shows that the PAPR of GFDM using 1st Xia filter and 4th Xia filter are almost the same, with the PAPR of 15.4 dB, lower than the other filters. However, RRC filter has the highest PAPR of 15.8 dB followed by RC filter with a PAPR of 15.5 dB, which concludes that when the CCDF is lower than 0.2, the GFDM system using RRC filter is higher than RC filter by 0.3 dB.

Figure 9 shows the PAPR of GFDM communication system of RC filter with different roll-off factor α. The increase

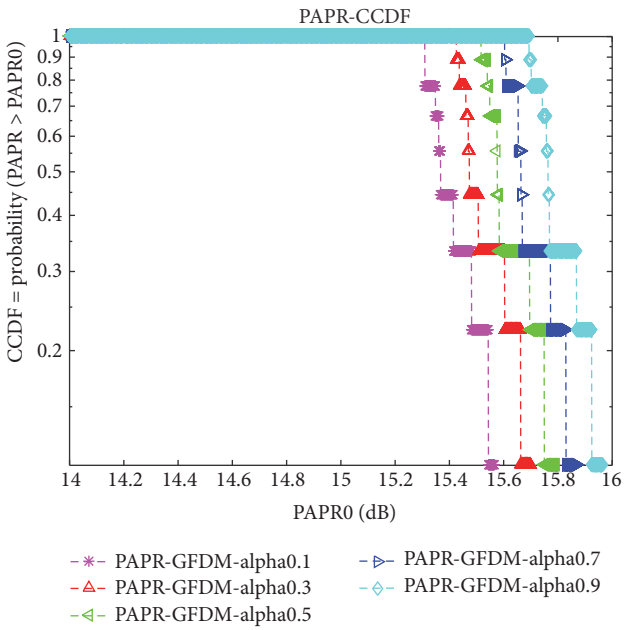

Figure 9: CCDF of GFDM communication system with different α.

step of roll-off factor α is 0.2. When the roll-off factor α equals 0.9, the PAPR of GFDM system is 0.4 dB higher than the case when α equals 0.1. Obviously, the PAPR of GFDM increases with the increase in roll-off factor α. Whenever α rises by one step, the PAPR will increase by 0.1 dB. The results prove that the selection of the pulse shaping filter has a great influence on the performance of GFDM communication system. Thus, PAPR is influenced by either the same filter with different roll-off factors α or different filters with the same roll-off factor.

4. Conclusion

In this paper, we investigated the influence of pulse shaping filters on the PAPR of the GFDM system. GFDM is an emerging candidate for future 5G networks. Taking advantage of the high degree of flexibility in frequency band selection, it apparently seems more suitable for the bandwidth limited UWA systems. The multicarrier scheme has both the advantage of making full use of the fragment spectrum and the merit of low PAPR, which will reduce the power consumption and save the hardware cost. The detailed PAPR of GFDM is analyzed. Different block structures, different filters, and different roll-off factors are factors that influence the PAPR of GFDM.

However, foreseen scenarios for future 5G networks have requirements that undoubtedly go beyond higher data rates. Because of the flexibility of GFDM, it becomes a promising solution for 5G communication and can satisfy diverse requirements. This paper gives a systematical analysis and it is an important reference for further application of this technique about how to select the appropriate filter banks and parameters according to the linear dynamic range of the transmitter power amplifier. The research of the application of algorithms developed for OFDM in underwater acoustic

GFDM, as well as other filters which can restrain the PAPR, will be the further research.

Competing Interests

The authors declare that they have no competing interests.

Acknowledgments

The authors thank the National Natural Science Foundation of China (Project nos. 61431004, 6140114, 11274079, and 61601137).

References

[1] T. Ihalainen, A. Viholainen, T. H. Stitz, and M. Renfors, "Generation of filter bank-based multicarrier waveform using partial synthesis and time domain interpolation," *IEEE Transactions on Circuits and Systems. I. Regular Papers*, vol. 57, no. 7, pp. 1767–1778, 2010.

[2] G. Fettweis, M. Krondorf, and S. Bittner, "GFDM—generalized frequency division multiplexing," in *Proceedings of the IEEE 69th Vehicular Technology Conference (VTC '09)*, pp. 1–4, IEEE, Barcelona, Spain, April 2009.

[3] X.-G. Xia, "A family of pulse-shaping filters with ISI-free matched and unmatched filter properties," *IEEE Transactions on Communications*, vol. 45, no. 10, pp. 1157–1158, 1997.

[4] N. Michailow, I. Gaspar, S. Krone, M. Lentmaier, and G. Fettweis, "Generalized frequency division multiplexing: analysis of an alternative multi-carrier technique for next generation cellular systems," in *Proceedings of the 9th International Symposium on Wireless Communication Systems (ISWCS '12)*, Paris, France, August 2012.

[5] G. Fettweis and S. Alamouti, "5G: personal mobile internet beyond what cellular did to telephony," *IEEE Communications Magazine*, vol. 52, no. 2, pp. 140–145, 2014.

[6] G. Wunder, P. Jung, M. Kasparick et al., "5GNOW: non-orthogonal, asynchronous waveforms for future mobile applications," *IEEE Communications Magazine*, vol. 52, no. 2, pp. 97–105, 2014.

[7] N. Michailow, S. Krone, M. Lentmaier, and G. Fettweis, "Bit error rate performance of generalized frequency division multiplexing," in *Proceedings of the 76th IEEE Vehicular Technology Conference (VTC Fall '12)*, pp. 1–5, September 2012.

[8] N. Michailow, M. Matthe, I. S. Gaspar et al., "Generalized frequency division multiplexing for 5th generation cellular networks," *IEEE Transactions on Communications*, vol. 62, no. 9, pp. 3045–3061, 2014.

[9] F. Schaich and T. Wild, "Waveform contenders for 5G—OFDM vs. FBMC vs. UFMC," in *Proceedings of the 6th International Symposium on Communications, Control and Signal Processing (ISCCSP '14)*, pp. 457–460, IEEE, Athens, Greece, May 2014.

[10] F. Boccardi, R. Heath Jr., A. Lozano, T. L. Marzetta, and P. Popovski, "Five disruptive technology directions for 5G," *IEEE Communications Magazine*, vol. 52, no. 2, pp. 74–80, 2014.

[11] S. Morosi, M. Biagini, F. Argenti, E. Del Re, and L. Yessenturayeva, "Frame design for 5G multicarrier modulations," in *Proceedings of the 11th International Wireless Communications and Mobile Computing Conference (IWCMC '15)*, pp. 1000–1005, August 2015.

[12] P. Banelli, S. Buzzi, G. Colavolpe, A. Modenini, F. Rusek, and A. Ugolini, "Modulation formats and waveforms for 5G networks: who will be the heir of OFDM?: an overview of alternative modulation schemes for improved spectral efficiency," *IEEE Signal Processing Magazine*, vol. 31, no. 6, pp. 80–93, 2014.

[13] M. A. A. Ali, "5G transceiver filters," in *Proceedings of the Conference of Basic Sciences and Engineering Studies (SGCAC '16)*, pp. 121–126, IEEE, Khartoum, Sudan, February 2016.

[14] J. Bazzi, P. Weitkemper, K. Kusume, A. Benjebbour, and Y. Kishiyama, "Design and performance tradeoffs of alternative multi-carrier waveforms for 5G," in *Proceedings of the IEEE Globecom Workshops (GC Wkshps '15)*, pp. 1–6, IEEE, San Diego, Calif, USA, December 2015.